Ignan Earths: Habitability of Terrestrial Planets with Extreme Internal Heating

Matthew Reinhold[1], **Laura Schaefer**[2]

[1,2]Stanford University

Key Points:

- Terrestrial planets with extreme internal heating exhibit rheologically solid mantles, and thus stable crusts.
- These planets should exhibit negative climate feedbacks, allowing for habitable surface temperatures to be maintained over geologic time.
- Wide ranges of heating rates yield temperatures similar those Earth has experienced in the past, meaning Ignan Earths should be habitable.

Corresponding author: Matthew Reinhold, `mackreth@stanford.edu`

Abstract

Is it possible for a rocky planet to have too much internal heating to maintain a habitable surface environment? In the Solar System, the best example of a world with high internal heating is Jupiter's moon Io, which has a heat flux of approximately 2 W m^{-2} compared to the Earth's 90 mW m^{-2}. The ultimate upper limit to internal heating rates is the Tidal Venus Limit, where the geothermal heat flux exceeds the Runaway Greenhouse Limit of 300 W m^{-2} for an Earth-mass planet. Between Io and a Tidal Venus there is a wide range of internal heating rates whose effects on planetary habitability remain unexplored. We investigate the habitability of these worlds, referred to as Ignan Earth's. We demonstrate how the mantle will remain largely solid despite high internal heating, allowing for the formation of a convectively buoyant and stable crust. In addition, we model the long-term climate of Ignan Earth's by simulating the carbonate-silicate cycle in a vertical tectonic regime (known as heat-pipe tectonics, expected to dominate on such worlds) at varying amounts of internal heating. We find that Earth-mass planets with internal heating fluxes below 30 W m^{-2} produce average surface temperatures that Earth has experienced in its past (below 30 °C), and worlds with higher heat fluxes still result in surface temperatures far below that of 100 °C, indicating a wide range of internal heating rates may be conducive with habitability.

Plain Language Summary

Greenhouse gases are naturally put into Earth's atmosphere by volcanoes, and taken out by rain, incorporating them into the rocks of Earth's tectonic plates, which then sink back into the Earth's interior. This cycle keeps our planet comfortable for life. However, this cycle needs a hot planetary interior to function. If a planet's internal heating is too low, this cycle shuts down resulting in a dead world, as can be see in the planet Mars. What about the other extreme? Could a planet sustain life if its interior were heated far more than the Earth? We call these worlds Ignan Earths and find that they should have solid interiors with stable crusts. However, their crusts will experience continuous volcanic activity, releasing greenhouse gases and reshaping the surface. We explore the buildup of these gases in the atmosphere, investigate the resulting climate, and find that Ignan Earths should have surface temperatures similar to those Earth has experienced in the past, meaning these planets should be able to support life.

1 Introduction

A habitable planet like the Earth requires active geology to maintain a temperate climate over long timescales (Kasting et al., 1993). In order to power such geologic processes, the planetary interior must have sufficient heat. The question then arises as to how much heating can a terrestrial world experience before it is rendered uninhabitable? Barnes et al. (2009) takes the upper limit to be comparable to the heating rate of Jupiter's moon Io (around 2 W m^{-2} (Lainey et al., 2009)), as it is generally assumed that a world with the volcanism rate of Io could not support the development of life. However, this assumption remains untested. The absolute maximum upper limit is where the internal heating rate will trigger a runaway greenhouse, known as the Tidal Venus Limit described by Barnes et al. (2013). A runaway greenhouse occurs when the total energy flux into the atmosphere of a planet (the sum of stellar insolation and geothermal heat) is sufficient to initiate a positive feedback loop between the evaporation of water and the resulting increase in the planetary greenhouse effect (Nakajima et al., 1992; Goldblatt & Watson, 2012). Calculated values of this flux range from 285 to 310 W m^{-2}, with a value of 300 W m^{-2} being generally accepted (Selsis et al., 2007; Barnes et al., 2013). The difference between the assumed limit and the definitive limit (Io's 2 W m^{-2} and the Tidal Venus's 300 W m^{-2}) is vast, encompassing a wide range of heating rates in potential terrestrial planets (generally referred to as Super Io's) whose habitability remains

unexplored. The subset of Super Io's that are potentially habitable will be referred to from here on as Ignan Earth's.

For rocky worlds, there are numerous sources to provide internal heat, including the energy received during planetary accretion, the latent heat of crystallization of the core and the decay of radioactive isotopes (Solomatov, 2007). However, none of these are able to produce and sustain the internal heating necessary for a Super Io, and thus an Ignan Earth. One source of heating that could be sufficient is that caused by tidal dissipation. Tidal heating can raise the average geothermal heat flux of a rocky world by orders of magnitude, such as the 2 W m^{-2} of Io (Lainey et al., 2009; Barr et al., 2018). The magnitude of tidal heating within a body is dependent on the size of the body, mean orbital motion, eccentricity and compositional properties (Murray & Dermott, 2000). The orbital periods for planets in habitable zones around Sun-like stars are too long for any significant tidal heating due to stellar tides. However, the majority of stars in the Universe are low mass M-dwarfs. Planets within the habitable zones of such stars have very short orbits, as red dwarfs have very low stellar luminosities (Shields et al., 2016). In fact, tidal heating should dominate the internal heat budget of planets in the habitable zone around stars less than 0.3 $M_\odot$ (Driscoll & Barnes, 2015). Therefore, we expect that most Ignan Earths in the Universe will be orbiting M-dwarfs. In addition, M-dwarf stars are fully convective and therefore produce strong magnetic fields, which any Ignan Earth will be orbiting through. Any such planets with an orbit inclined to their star's magnetic dipole will experience continuously changing magnetic fields within the planet's mantle. The eddy currents generated would dissipate as heat, adding to the planet's internal heat budget. Kislyakova et al. (2018) suggests that this magnetic induction heating could be a significant internal heat source for such planets.

In this paper we investigate the habitability of Ignan Earths. This required the use of two independent models: One for determining the nature of the mantle and thus the stability of the crust (see Sec. 2), and the other for modeling the the atmosphere-interior coupling and simulating the resulting climate (see Sec. 3). Each of these models has their own methods and results section along with their own sets of terms found in their own respective tables. The terms in each section applies to their section only.

In Sec. 2, we determine if the mantle of an Ignan Earth behaves as a liquid or a solid, and subsequently assess the long term stability of the crust. In order for a planetary surface to be habitable, the crust needs to be stable, persisting for timescales long enough for ecological communities to gain a foothold. Crust formation on a planet with a solid mantle is caused by the eruption and buildup of partial melt from within onto the surface. This crust is less dense than the underlying mantle and thus remains buoyant. However, the buoyancy of any solid crust over a liquid mantle is less certain.

Once we establish the buoyancy and stability of the crust, we investigate the nature of the tectonic regime of an Ignan Earth, as they are likely to be very unlike classical terrestrial planets. Earth experiences a mobile lid plate tectonic regime that works to recycle old oceanic crust (Davies, 2007), as opposed to Mars and Venus where no fracturing or large scale recycling of the crust is evident. This is known as a stagnant lid tectonic regime (O'Neill & Roberts, 2018). Worlds with partially molten mantles are expected to experience a different tectonic regime known as heat-pipe tectonics, known to dominate on Io (O'Reilly & Davies, 1981; Moore & Webb, 2013). Melt is erupted onto the surface and builds up, forcing the older layers down, causing a vertical recycling of the crust. It is this advection of melt to the surface that is the primary mechanism of heat transport through the crust, as opposed to conduction. Evidence for advection of heat can be seen not only on Io, but also at Earth's mid-ocean ridges, where our planet experiences the highest geothermal heat flux and where the majority of this heat is transported up through hydrothermal fluids and vents (Fontaine et al., 2011; Sleep et al., 2014). It is therefore reasonable to assume that heat-pipe tectonics and vertical recycling may be common on worlds where geothermal heat fluxes are high, such as Ignan Earths.

In Sec. 3, we couple the mantle with the atmosphere using a heat-pipe tectonic regime to determine the resulting atmospheric composition. We will then combine the stellar flux and the high geothermal flux with the resultant atmosphere in climate models to determine average surface temperature to characterize planetary habitability. Finally, in Sec. 4, we examine the circumstellar and planetary environments where Ignan Earths could exist, and explore some possible Ignan Earth candidates among known exoplanets.

2 Mantle and Crust

In the following section, we describe a magma ocean thermal evolution model which we use to explore the mantle rheology and crustal stability of Ignan Earths. We then discuss results from our model and how they vary with respect to planet mass. All constants for this section are displayed in Table 1.

2.1 Methods

Earth's internal heat is transported through mantle convection, meaning the mantle temperature profile follows an adiabatic gradient. This adiabat lies below the solidus, thus the mantle is entirely solid (Solomatov, 2007). Partial melting does occur, but it is limited to volcanic centers like mid-ocean ridges and hot spots, where melting is driven by adiabatic decompression of rising mantle material (Davies, 2007). However, worlds with higher internal heating rates will have higher temperature adiabats and thus the potential for permanent partial melt regions within their mantles. Observations suggest that Io has a subsurface layer of mantle over 50 km deep with a melt fraction of up to 0.2 (Khurana et al., 2011) and therefore it is reasonable to assume that the presence of permanent partial melt layers may be common on Ignan Earths.

We simulate the thermal evolution of the mantle for a terrestrial planet and allow it to come to a steady state. This is modeled by modifying the internal evolution models for magma oceans described by Schaefer et al. (2016). The mantle thermal evolution is determined by calculating the upper mantle potential temperature using

$$\frac{dT_{man}}{dt} = \frac{\rho_m \pi Q_r (R_p^3 - R_c^3) - 3\pi R_p^2 q_m}{\rho_m \pi c_p (R_p^3 - R_c^3)} \tag{1}$$

were Q_r is the total internal heat generated, q_m is the heat flux through the surface, ρ_m is the mantle density, c_p is the silicate heat capacity, and R_p and R_c are the planet and core radii, respectively. With this, we can calculate the thermal evolution of a rocky planet from a fully molten magma ocean through crystallization and subsequent solid-state convection. Internal heating Q_r, is assumed to occur uniformly throughout the planet, with each kilogram having a specific heat production term. This will be set as the sum of an Earth-like radiogenic heating component and an arbitrarily specified heating value.

$$Q_r = q_\oplus + Q_{extra} \tag{2}$$

were $q_\oplus$ is the modern Earth's heat production and Q_{extra} is the arbitrarily specified heating value, ranging from 0 W kg^{-1} up to 3.91×10^{-8} W kg^{-1} (for an Earth-mass planet), equivalent to the geothermally induced runaway greenhouse described by Barnes et al. (2013). We assume both of these heat production terms are confined to the mantle only. The heat flux through the surface, q_m, is dependent on both the mantle below and the atmosphere above. To fully capture this term, we must not only model mantle evolution, but the resulting planetary atmosphere as well. To do this, we use the model set forth by Elkins-Tanton (2008).

As the magma ocean cools, it degases any volatiles that exceed the magma's saturation limit. We determine the atmospheric partial pressures of the relevant greenhouse gases carbon dioxide P_{CO_2} and water vapor P_{H_2O}:

$$P_{H_2O} = \left(\frac{H_2O_{mag}(wt\%) - 0.3}{2.08 \times 10^{-4}} \right)^{\frac{1}{0.52}} [Pa] \tag{3}$$

$$P_{CO_2} = \left(\frac{CO_{2mag}(wt\%) - 0.05}{2.08 \times 10^{-4}} \right)^{\frac{1}{0.45}} [Pa] \tag{4}$$

Each are calculated from the saturation weight percent of water and CO_2 (H_2O_{mag} and CO_{2mag}, respectively) in a magma ocean equilibrated to an atmosphere with an assumed initial surface pressure of 1 bar. Our assumed H_2O_{mag} weight percent (see Table 1), applied to the entire mantle, would result in 1.48×10^{22} kg of H_2O, or 10.7 earth oceans of water in the mantle. For the modern Earth, estimates for mantle water capacity range from approximately one ocean in the upper mantle (Fei et al., 2017), up to three oceans in the transition zone (Nishi et al., 2014; Schmandt et al., 2014) and possibly four oceans in the lower mantle (Peslier et al., 2017). However, estimates for the total abundance of water within the Earth have a wide range, with Hirschmann (2018) suggesting only 2 oceans worth, while Marty (2012) estimates approximately 11.7 oceans worth. Our estimate therefore falls within these extremes, and therefore we surmise it to be a reasonable estimate. Similarly, our assumed CO_{2mag} also falls within the independently estimated extremes. We calculate a CO_2 content in the mantle of 3.62×10^{21} kg. Hirschmann (2018) estimates 5.56×10^{20} kg of C, which would translate to 2.04×10^{21} of CO_2, while Marty (2012) estimates 3.14×10^{21} kg of C, which would translate to 1.15×10^{22} of CO_2.

We now calculate the partial atmospheric mass of each species i (H_2O and CO_2) as described by Bower et al. (2019)

$$M_{atm_i} = \frac{4\pi R_p^2 P_i}{g} \left(\frac{\mu_i}{\bar{\mu}} \right) \tag{5}$$

where g is the acceleration due to gravity, $\bar{\mu}$ is the mean molar mass of the atmosphere, and P_i and μ_i are the surface partial pressure and molar mass of species i. To find how easily heat escapes this atmosphere to space, we calculate the optical depth for each species

$$\tau_i = \left(\frac{3M_{atm_i}}{8\pi R_p^2} \right) \left(\frac{k_i g}{3P_{ref}} \right)^{\frac{1}{2}} \tag{6}$$

where k_i is the atmospheric absorption coefficient for species i at a set reference pressure of P_{ref}. Using the full optical depth $\tau = \sum \tau_i = \tau_{H_2O} + \tau_{CO_2}$, we determine the atmospheric emissivity

$$\epsilon = \frac{2}{\tau + 2} \tag{7}$$

Assuming the atmosphere is a grey radiator with no convective heat transport, we can use the emissivity to calculate the heat flux out of the atmosphere to space

$$q_a = \epsilon\sigma \left(T_{surf}^4 - T_{eq}^4 \right) \tag{8}$$

where T_{surf} is the surface temperature and T_{eq} is the equilibrium blackbody temperature of the planet, described by

$$T_{eq} = \left[\left(\frac{S(1-A)}{4} + q_m \right) \left(\frac{1}{\sigma} \right) \right]^{\frac{1}{4}} \tag{9}$$

where S is the solar constant, A is the planetary albedo and σ is the Stefan-Boltzmann constant.

Finally, we can calculate the surface temperatures for varying internal heating rates using

$$\frac{dT_{surf}}{dt} = \frac{4\pi R_p^2 (q_m - q_a)}{M_{atm} C_{p,H_2O} + \frac{4}{3} c_p \pi \rho_m (R_p^3 - l^3)} \tag{10}$$

where C_{p,H_2O} is the thermal capacity of water vapor and l is the thermal boundary layer (defined below). We find surface temperatures of 255 K for no additional heating, ranging up to over 400 K for extreme heating rates. These temperatures depend on the resulting water and CO_2 atmospheric concentrations, which are dependent of the initial H_2O_{mag} and CO_{2mag} weight percents specified in Eq. 3 and Eq. 4. These weight percents are based on their saturation values for a given atmospheric pressure. The higher the initial atmospheric pressures, the higher the resulting surface temperatures. For example, assuming an initial 10 bar atmosphere results in a surface temperature range from 259 K up to 770 K.

The thermal boundary layer is defined by

$$l = \frac{k \Delta T}{q_m} \tag{11}$$

where $\Delta T = T_{man} - T_{surf}$ and k is the thermal conductivity of the mantle. Equations 1, 10 and 11 all are dependent on the surface heat flux out of the mantle

$$q_m = \left(\frac{k \Delta T}{D_{man}} \right) \left(\frac{Ra}{Ra_c} \right)^{\beta} \tag{12}$$

where Ra and Ra_c are the Rayleigh and Critical Rayleigh Numbers, respectively, whose ratio is raised to a scaling factor β. D_{man} is the depth of the convecting mantle layer. During magma ocean crystallization, it is likely that two-layer convection did occur as the mantle crystallized from the bottom up (Maurice et al., 2017; Boukaré et al., 2018; Morison et al., 2019). However, we are interested in the nature of the mantle at a final steady-state where the entire mantle will be rheologically homogeneous. Therefore we assume the depth of the convecting layer D_{man} is equal to the thickness of the entire mantle

The Rayleigh Number describes the vigor of convection and is calculated by

$$Ra = \frac{\alpha g \Delta T D_{man}^3}{\kappa \nu} \tag{13}$$

where α is the thermal expansion coefficient, κ is the thermal diffusivity and ν is the kinematic viscosity. To find the kinematic viscosity, we need to understand the rheology of the mantle throughout the cooling process. A liquid mantle will cool quickly as it experiences rapid convection due to the low viscosities of its liquid rheology and high temperatures. When the liquid mantle begins to crystallize, solids are introduced into the system, and eventually the mantle rheology will change from a liquid to a solid. This rheology depends on the melt fraction within, described by

$$\phi = \frac{T_{man} - T_{sol}}{T_{liq} - T_{sol}} \tag{14}$$

where T_{sol}, T_{liq} and T_{man} are the solidus, liquidus and upper mantle potential temperatures, respectively (Lebrun et al., 2013). We use the upper liquidus and solidus temperatures shown in Abe (1997); Lebrun et al. (2013), where $T_{liq} = 2000$ K and $T_{sol} = 1400$ K.

With the solidus and liquidus temperatures specified, we can calculate the melt fraction of the mantle, and from that the viscosity. Melt fraction ranges from 0 (completely solid) to 1 (completely liquid) with the viscosity transition occurring at the critical value of $\phi_c = 0.4$. Above this threshold, solid particles loose connectivity allowing the mantle to behave as a liquid, while below ϕ_c solid particles retain connectivity, making the mantle rigid and thus a solid. We simulate the changing viscosity of liquid convection to solid convection using different viscosity formulations, as described by Lebrun et al. (2013). For liquid convection the dynamic viscosity is

$$\eta = \frac{\eta_l}{\left(1 - \frac{1-\phi}{1-\phi_c}\right)^{2.5}} \tag{15}$$

where

$$\eta_l = A_1 \exp\left(\frac{B}{T_{man} - 1000}\right) \tag{16}$$

where A_1 and B are empirical, material dependent parameters given in Table 1. For solid convection the dynamic viscosity is

$$\eta = \eta_s \exp(-\alpha_n \phi) \tag{17}$$

where α_n is a constant dependent on the creep mechanism and η_s is described by

$$\eta_s = \frac{\mu}{2A_2}\left(\frac{h}{b}\right)^{2.5} \exp\left(\frac{E}{RT_{man}}\right) \tag{18}$$

where μ is the shear modulus, h is the grain size, A_2 is the pre-exponential factor, b is the Burger vector length, R is the universal gas constant and E is the activation energy. We then find the kinematic viscosity

$$\nu = \frac{\eta}{\rho_m} \tag{19}$$

where η is the dynamic viscosity of either a liquid or a solid rheology, calculated in Eq. 15 or Eq. 17, respectively. This kinematic viscosity is used in calculating the Rayleigh Number in Eq. 13

The melt fraction ϕ is calculated for each simulated Ignan Earth to determine the mantle rheology. Understanding this rheology is critical for understanding the buoyancy of the crust and thus the planet's habitability. If the mantle behaves as a liquid, the mantle at the surface will cool to form a solid quench crust which will have the same composition as the liquid mantle below. This crust will be negatively buoyant and will founder into the mantle almost immediately, rendering the planet uninhabitable. If the mantle behaves as a solid, any crust that forms on the surface has the potential to be positively

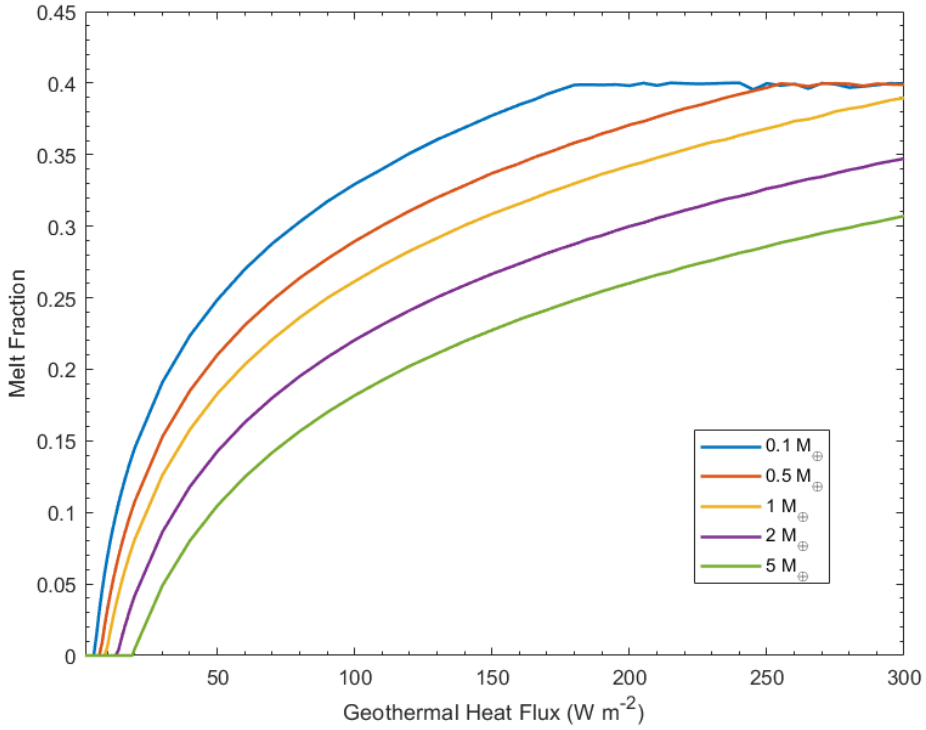

Figure 1. Melt fraction of the mantle for planets with masses ranging from 0.1 - 5 $M_\oplus$ for geothermal heat fluxes between 2 - 300 W m^{-2}.

buoyant and stable over geologic time (like Earth's crust), thus allowing for habitability.

2.2 Mantle and Crust - Results

The equilibrium upper mantle temperatures and mantle melt fractions are determined for geothermal heat fluxes ranging from $2-300\ W/m^2$ for planet masses ranging from $0.1{-}5\ M_\oplus$, shown in Fig. 1. The parameters of each planet are calculated based on the work by Zeng et al. (2019) and are displayed in Table 2. We find that even at Tidal Venus limits of heating ($300\ W/m^2$), the melt fraction of the mantle never rises above the critical value of 0.4, meaning the mantle will remain in a solid rheological state. For the lowest mass planets, the critical melt fraction of 0.4 is reached but never surpassed. The reason for this is that viscosities are low in the liquid regime, allowing for vigorous convection and rapid heat loss, far surpassing any heat production within. If the mantle ever finds itself in this regime, it will rapidly cool off until the mantle reaches the solid regime, where an equilibrium between heat loss and heat production is possible. Note that these results are consistent with the work of Lebrun et al. (2013), who find heat fluxes similar to the Tidal Venus limit for the transition from partially molten ($\phi > 0.4$) to "mush" stage ($\phi \leq 0.4$), depending on the radiative transfer model used for atmospheric heat loss. They also find that fully molten magma oceans produce heat fluxes of order 10^5 - 10^7 W m^{-2}, well above the Tidal Venus limit. Therefore, the mantles of all Ignan Earth's will have melt fractions of 0.4 or less and exhibit a solid rheology. With a solid mantle, a planetary crust will be able to form by the same process as on Earth: The eruption of partial melts from below. As partial melts are compositionally distinct from the

Table 1. Parameters used in mantle thermal evolution model described in Sec. 2.

Parameter	Symbol	Value	Units
Earth Mass	$M_\oplus$	5.97×10^{24}	kg
Core Radius	R_c	3.48×10^6	m
Planet Radius	R_p	6.37×10^6	m
Grav. Acceleration	g	9.8	m s^{-2}
Planet density	$\rho_\oplus$	5510	kg m^{-3}
Mantle density	ρ_m	4000	kg m^{-3}
Mantle specific heat	c_p	1000	J kg^{-1} K^{-1}
Initial water content of mantle	H_2O_{mag}	0.37	wt%
Initial carbon dioxide content of mantle	CO_{2mag}	0.09	wt%
Specific heat of water vapor	C_{p,H_2O}	1990	J kg^{-1} K^{-1}
Absorption coefficient of water	k_{H_2O}	0.01	m^2 kg^{-1}
Absorption coefficient of carbon dioxide	k_{CO_2}	0.05	m^2 kg^{-1}
Reference pressure	P_{ref}	1×10^5	Pa
Atmospheric mean molar mass	$\bar{\mu}$	28.97	g $mol^{-}1$
Molar mass of water vapor	μ_{H_2O}	18.02	g $mol^{-}1$
Molar mass of carbon dioxide	μ_{CO_2}	44.01	g $mol^{-}1$
Planetary albedo	A	0.3	
Solar constant	S	1360	W m^{-2}
Earth modern heat production	$q_\oplus$	1.17×10^{-11}	W kg^{-1}
Thermal conductivity	k	4.2	W m^{-1} K^{-1}
Thermal diffusivity	κ	1×10^{-6}	m^2 s^{-1}
Thermal expansion coefficient	α	2×10^{-5}	K^{-1}
Critical Rayleigh Number	Ra_c	1000	
Liquidus Temperature	T_{liq}	2000	K
Solidus Temperature	T_{sol}	1400	K
Critical melt fraction	ϕ_c	0.4	
Empirical constant	A_1	2.4×10^{-4}	Pa
Empirical constant	B	4600	K
Creep constant	α_n	26	
Shear modulus	μ	8×10^{10}	Pa
Grain size	h	0.01	m
Burger vector length	b	5×10^{-10}	m
Pre-exponential factor	A_2	5.3×10^{15}	
Activation energy	E	3×10^5	J kg^{-1}

bulk mantle, the resulting solid crust will also be compositionally distinct from the mantle, meaning the crust will likely be positively buoyant and therefore stable.

Our simulations are designed to model an evolving magma ocean and assumes an instantaneous exchange of volatiles between the mantle and atmosphere. Realistically, the concentration of water and CO_2 in the silicate liquid will change as the magma ocean solidifies, but we neglect this evolution for simplicity. However, the goal with our model is to determine the rheology of the mantle of an Ignan Earth during a steady state, not to accurately simulate an evolving magma ocean and resulting planetary atmosphere. While we have made a number of simplifying assumptions compared to the original volatile evolution model, we find that our results are robust to changes of H_2O and CO_2 abundances in melt across a range of values that would be encountered in an evolution model. What is important is the predicted rheological behavior of the mantle: Even when internal heating reaches extreme levels, the critical melt fraction will always remain at or

$M_\oplus$	R_c	R_p	g	ρ
0.1	0.508	0.515	0.395	0.766
0.5	0.694	0.833	0.771	0.927
1	1	1	1	1
2	1.223	1.123	1.590	1.158
5	1.602	1.524	2.143	1.482

Table 2. Planet properties used for Fig. 1. Each value (planet mass, core radius, planet radius, gravitational acceleration and average density) is normalized to the Earth, and was calculated using the work of Zeng et al. (2019).

below the critical value of 0.4, due to the negative feedback loop of mantle viscosity, temperature and convective heat loss. Therefore the mantle remains rheologically solid, allowing for a stable crust.

3 Ignan Earth Climate

In this section, we first provide a detailed discussion of a coupled atmosphere-crust-mantle vertical tectonic model which we use to explore the climatic habitability of Ignan Earths. We then discuss results from our nominal model and how our results vary by using different assumptions for seafloor weathering, stellar insolation, stellar spectrum, planet mass, total carbon budget and land fraction. Finally, we explore the types of environments where such Ignan Earth's might be found, and look at potential Ignan Earth candidates among known exoplanets. All constants for this section are displayed in Table 3.

3.1 Methods

The long-term habitability of a terrestrial planet is generally simulated by modeling the carbonate-silicate climate feedback. On Earth, CO_2 is pulled from the atmosphere through rain and consequently weathers silicate minerals in the crust and ocean floor. These carbonate rocks produced from weathering reactions are then subducted into the mantle and CO_2 is then degassed back into the atmosphere through volcanism. As surface weathering is temperature dependent, a temperate climate is maintained on Earth through this negative feedback cycle (Walker et al., 1981; Berner et al., 1983; Kasting et al., 1993). On an Ignan Earth, a similar feedback should operate, except with vertical heat-pipe tectonics in place of mobile lid plate tectonics.

We adopt the model of Valencia et al. (2018) to simulate the carbonate-silicate cycle on an Ignan Earth with vertical cycling. We start by assuming the planet is covered entirely by a global ocean with oceanic crust and lithosphere. As a consequence, seafloor weathering will be the only mechanism drawing down atmospheric CO_2 levels (unlike the Earth, where weathering occurs on both the continents and the seafloor). The carbon is brought into the mantle by the vertical cycling and released back into the atmosphere by volcanism. As these processes are directly linked, the resurfacing rate and subsidence rate will be equal (O'Reilly & Davies, 1981). We will model the steady-state atmospheric composition as a balance of CO_2 outgassing and burial, tracking the carbon in each important reservoir: Mantle, basaltic crust, and atmosphere-ocean (labeled as pCO_2^{man}, pCO_2^{bas} and pCO_2^{atm+oc}, respectively). The rate at which CO_2 is changing in each reservoir is described by the following linked differential equations

$$\frac{d}{dt}pCO_2^{atm+oc} = D\left(pCO_2^{man}\right) - W\left(pCO_2^{atm}, T_s\right) \tag{20}$$

$$\frac{d}{dt}pCO_2^{man} = F\left(pCO_2^{bas}\right) - D\left(pCO_2^{man}\right) \tag{21}$$

$$\frac{d}{dt}pCO_2^{bas} = W\left(pCO_2^{atm}, T_s\right) - F\left(pCO_2^{atm}, T_s\right) \tag{22}$$

where D is the degassing rate from volcanism, W is the total weathering rate and F is the foundering rate at the base of the crust. Both the degassing and foundering rates are directly dependent on the resurfacing rate of basalt in the vertical cycling regime. Each of these are described in the subsections below.

3.1.1 Resurfacing Velocity

The resurfacing velocity is the rate at which the basaltic crust replenishes itself through volcanism. As we assume the planet is in steady-state, this rate is also equal to the subsidence rate, and is described by

$$v = \frac{q_m}{\rho_m(L_m + C_p\Delta T)} \tag{23}$$

where L_m and C_p are the latent and specific heat of the mantle, respectively, and $\Delta T = T_{melt} - T_s$, where T_{melt} is the temperature of the erupting melt. Typical resurfacing velocities range from under 20 mm yr^{-1} up to 320 mm yr^{-1} over the range of explored internal heat fluxes, compared to Earth's average spreading ridge velocity of 50 mm yr^{-1}.

3.1.2 Weathering

CO_2 is removed from the atmosphere-ocean reservoir by weathering, both on the seafloor and on the continents. The seafloor weathering rate depends on CO_2 concentrations in the water and the temperature of the deep ocean. The CO_2 concentration in the ocean is related to the atmospheric concentrations according to Eq. 34, and the ocean temperature is broadly related to the average surface temperature, therefore it is possible to calculate the seafloor weathering as a function of atmospheric temperature and CO_2 concentrations in the following way

$$W_{sea}(T_s) = \omega W_{sea}^E \left(\frac{pCO_2^{atm}}{p_E}\right)^{\alpha} \exp\left(\frac{E}{R}\left[\frac{1}{T_{eq}} - \frac{1}{T_s}\right]\right) \tag{24}$$

where R is the universal gas constant, E is the activation energy, P_E is the atmospheric equilibrium partial pressure of CO_2, α is a dimensionless scaling factor and W_{sea}^E is the baseline weathering rate. The term ω describes the possible dependence weathering may have on the resurfacing velocity. This term can be parameterized such that $\omega = \left(\frac{v}{v_\oplus}\right)^{\beta}$, where the resurfacing velocity v (Eq. 23) is normalized to the Earth's modern spreading ridge velocity $v_\oplus$, scaled by a factor of β. We set the ω term to be equal to 1, and in subsequent runs calculate ω with varying factors of β. These variations do not influence our results significantly and a full discussion of their implications can be seen in Sec. 5.

However, some studies suggest seafloor weathering of CO_2 may be dependent on the geothermal heat flow at the site of hydrothermal alteration rather than the temperature of the deep ocean (Alt & Teagle, 1999). In addition, if the rate of oceanic crust

formation is significantly slower than the weathering process, then the weathering rate is limited by the supply of fresh basalt and not the kinetics of the reaction itself. This would result in temperature-independent seafloor weathering. We explore its effects using the model described by Foley (2015), where the temperature component is neglected

$$W_{sea} = \omega W^E_{sea} \left(\frac{pCO_2^{atm}}{p_E} \right)^{\alpha} \tag{25}$$

To simulate continental weathering we also use the model described by Foley (2015). If there is little exposed land, low erosion rates or high weathering rates, weathering is limited by the supply of fresh continental rocks at the surface. This supply-limited weathering is described by

$$W_{sup} = \frac{A_p f_l E_{rate} \chi_{cc} \rho_{cont}}{m_{cc}} \tag{26}$$

where E_{rate} is the physical erosion rate, f_l is the exposed land fraction of the planet, χ_{cc} is the fraction of reactable ions in the crust, ρ_{cont} is the density of the exposed continental surface crust and m_{cc} is the average molar mass of reactable elements available for reaction within the exposed crust.

When the supply of fresh rock to the surface is substantial enough the limiting factor is the kinetics of the weathering reaction itself. This kinetically-limited weathering is described by

$$W_{kin} = W^E_{kin} \left(\frac{pCO_2^{atm}}{p_E} \right)^{\delta} \left(\frac{P_{sat}}{P^*_{sat}} \right)^{\gamma} \exp\left(\frac{E}{R} \left[\frac{1}{T_{eq}} - \frac{1}{T_s} \right] \right) \left(\frac{f_l}{f^*_l} \right) \tag{27}$$

where W^E_{kin} is the reference continental weathering rate, f^*_l is the land fraction of the modern Earth, P^*_{sat} is the reference saturation vapor pressure of H_2O, and δ and γ are silicate weathering scaling factors for the atmospheric CO_2 and saturation vapor pressure ratios, respectively. The saturation vapor pressure can be found by

$$P_{sat} = P^*_{sat} \exp\left[-\frac{\mu_{H_2O} L_w}{R} \left(\frac{1}{T_s} - \frac{1}{T_{sat}} \right) \right] \tag{28}$$

where L_w is the latent heat of water and T_{sat} is the temperature for the reference saturation vapor pressure P^*_{sat}. To find a general description of continental weathering, the kinetically-limited and supply-limited rates are combined into the form

$$W_{cont} = W_{sup} \left(1 - \exp\left[-\frac{W_{kin}}{W_{sup}} \right] \right). \tag{29}$$

To find the overall weathering rate of CO_2, the continental and seafloor weathering rates are combined in the following manner

$$W = W_{cont} + (1 - f_l) W_{sea} \tag{30}$$

where the seafloor weathering term must be scaled by the fraction of the planet surface covered by ocean $(1 - f_l)$.

3.1.3 Foundering

Once the carbon from the atmosphere-ocean reservoir has been sequestered in the basaltic crust, the process of vertical cycling pushes that rock to the base of the crust where it delaminates and founders into the mantle. This foundering rate is given by

$$F = pCO_2^{bas}\left(\frac{v}{d_{bas}}\right) \tag{31}$$

where pCO_2^{bas} is the carbon content of the crustal basalt, v is the resurfacing velocity and d_{bas} is the thickness of the crust given by

$$d_{bas} = \frac{\kappa}{v} log\left(1 + \frac{kv}{\kappa}\frac{\Delta T}{q_{tot}(\frac{1}{a_q} - 1)}\right) \tag{32}$$

where κ and k are the thermal diffusivity and thermal conductivity, respectively, v is the resurfacing velocity (see Eq. 23), q_{tot} is the total geothermal heat flux, ΔT is the temperature difference between the surface and upper mantle, and a_q is the ratio of added heat to total internal heating, assuming the total heat is the sum of radioactive decay and artificially added heat. This yields varying thicknesses for different geothermal heat fluxes. Taking a low Q value of 1 W m^{-2} with a ΔT of 1250 K, a_q of 0.917, q_{tot} of 1.09 W m^{-2}, and a resurfacing velocity v of 2.18×10^{-10} m s^{-1} (6.9 mm yr^{-}1), we compute a crustal thickness d_{bas} of 4.5 km. For extreme values of Q, this thickness decreases to only a few hundred meters. We found that setting the thickness to a single value of 4 kilometers was sufficient for our models, as crustal thicknesses ranging from 5 - 0.1 km made no noticeable change to the final results.

3.1.4 Degassing Rate

CO_2 is returned from the mantle to the atmosphere through degassing during volcanic eruptions. The partial melt of the mantle buoyantly rises to the surface through the volcanic heat pipes and and degases the CO_2 to the atmosphere-ocean reservoir according to the following flux equation

$$D = pCO_2^{man}\left(\frac{f_{gas} v A_p}{V_{man}}\right) \tag{33}$$

where v is the resurfacing velocity, f_{gas} is the fraction of CO_2 outgassed, A_p is the surface area of the planet and V_{man} is the volume of the mantle.

3.1.5 Climate Model

Using Eq. 20 we find the CO_2 content of the atmosphere-ocean reservoir. To find the atmospheric content we calculate the partitioning of CO_2 between the atmosphere and the ocean

$$pCO_2^{atm} = \frac{K_H}{\mu_{co_2}}\frac{pCO_2^{oc}}{\left(\frac{pH_2O}{\mu_{H_2O}} + \frac{pCO_2^{oc}}{\mu_{CO_2}}\right)} \tag{34}$$

where K_H is the solubility constant, p_{H_2O} is the water content of the ocean expressed as an atmospheric pressure in bars, $p_{CO_2^{oc}}$ is the CO_2 content of the ocean and μ is the molar mass of each respective species.

With the atmospheric CO_2 calculated, the global climate can be modeled and an average surface temperature T_s is determined. This temperature is calculated by combining the effects of stellar insolation (we initially assume a modern day, Earth-analogous solar insolation) and geothermal heat flux, while accounting for the greenhouse effects of CO_2 and H_2O in the atmosphere. The equilibrium temperature of a planet is calculated from Eq. 9. To account for the effect of greenhouse gases, we relate atmospheric CO_2 content to surface temperature by the simple parameterization used in Foley (2015):

$$T_s = T_{ref} + 2(T_{eq} + T^*_{eq}) + 4.6 \left(\frac{pCO_2}{pCO^*_2} \right)^{0.346} - 4.6 \tag{35}$$

where T_s is the surface temperature, pCO_2 is the partial pressure of CO_2, T_{eq} is the effective temperature (calculated using Eq. 9), T^*_{eq} is the reference effective temperature, T_{ref} is reference surface temperature and pCO^*_2 is the reference partial pressure of CO_2. This is a first order approximation that accounts for the warming for both atmospheric CO_2 and H_2O (the atmosphere is assumed to always be saturated with water vapor), and reproduces the results of more sophisticated radiative-transfer models. However, it deviates under high CO_2 levels (approximately 10 bar or above), but as can be seen in Section 3.2, our predicted CO_2 levels never approach these values. We use this parameterization by Foley (2015) as it is built for terrestrial, Earth-like planets, whereas of the climate model described in Sec. 2 is built for evolving magma ocean planets.

3.2 Results

For an Earth-mass planet, the Runaway Greenhouse Limit is when the total planetary insolation reaches 300 W m^{-2}. For our initial model, we assume a total absorbed short wave solar flux equal to the modern Earth value of 240 W m^{-2}. Therefore, if the geothermal heat flux exceeds 60 W m^{-2}, the total insolation will exceed the Runaway Greenhouse Limit. As our climate model does not account for the Runaway Greenhouse, we use that value of 60 W m^{-2} as an artificial cutoff. Our baseline assumption is a planet completely covered in a global ocean where seafloor weathering is temperature-dependent, with an Earth-like planetary albedo and solar constant (0.3 and 1360 W m^{-2}, respectively). We calculate CO_2 concentrations and resulting average surface temperatures. In Fig. 2 we show the the results of our climate models for such a planet with geothermal heat flux values ranging from 2 - 60 W m^{-2}. Fig. 2a and Fig. 2b show the average surface temperature and atmospheric CO_2 content, respectively, for a given geothermal heat flux with the modern Earth's values given for reference. It is important to note that the predicted surface temperature for a given CO_2 concentration is distinctly higher that it would be on Earth due to the increased energy flux the atmosphere experiences from geothermal heat.

While the vast majority of model results predict Ignan Earth's to be warmer than modern Earth, almost all fall within temperature ranges Earth has experienced in it's past. Heat fluxes between 20 - 45 W m^{-2} yield average temperatures between 25 and 35 °C, similar to temperature estimates for multiple hyperthermal events in Earth's history, including the Late Cretaceous Period (O'Connor et al., 2019), the Paleocene-Eocene Thermal Maximum and the Eocene Climatic Optimum (Inglis et al., 2020). Heat fluxes less than 7 W m^{-2} predict Ignan Earths with global temperatures cooler than the modern value of 14 °C and similar to Earth's glacial periods, with Io-like heat fluxes predicting temperatures around 10 °C, close to the 8 °C of the Last Glacial Maximum (Tierney et al., 2020). The takeaway from this is that most predicted temperatures fall within ranges Earth has experienced during its history while life thrived, and thus these predicted surface temperatures should offer no barrier to the habitability of Ignan Earth's.

For a planet with exposed continents and temperature-dependent seafloor weathering, continental weathering will become important. We vary the land fraction f_l for

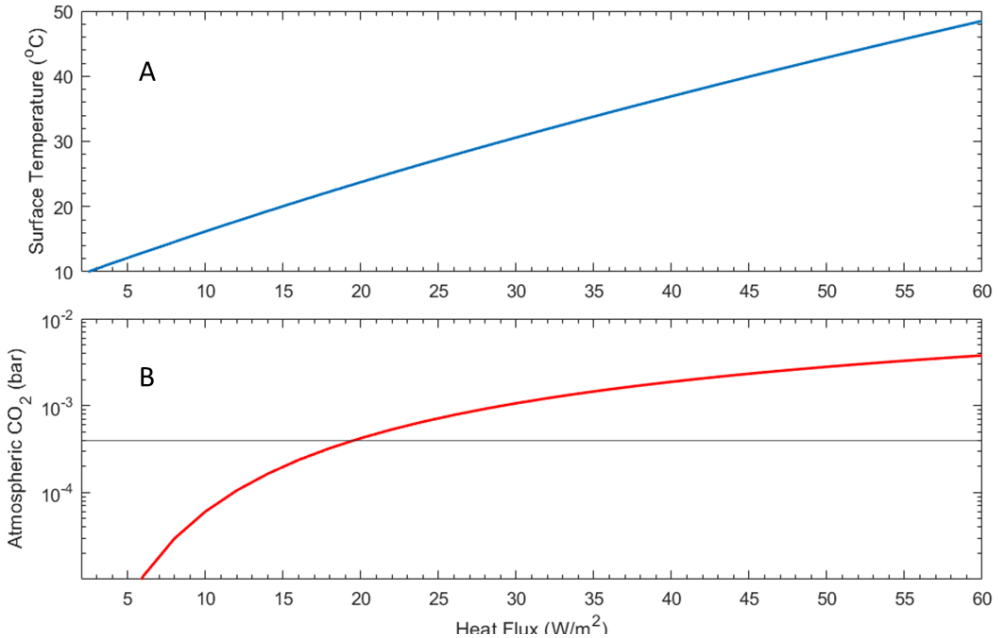

Figure 2. Average surface temperature (A) and atmospheric CO_2 (B) for a 1 $M_\oplus$ Ignan Earth for geothermal fluxes ranging up to 60 W m^{-2}. The black horizontal lines represent the modern Earth surface temperature and CO_2 partial pressures, for comparison. Beyond a geothermal heat flux of 60 W m^{-2}, the sum of solar insolation + geothermal heat flux exceeds the Runaway Greenhouse Limit.

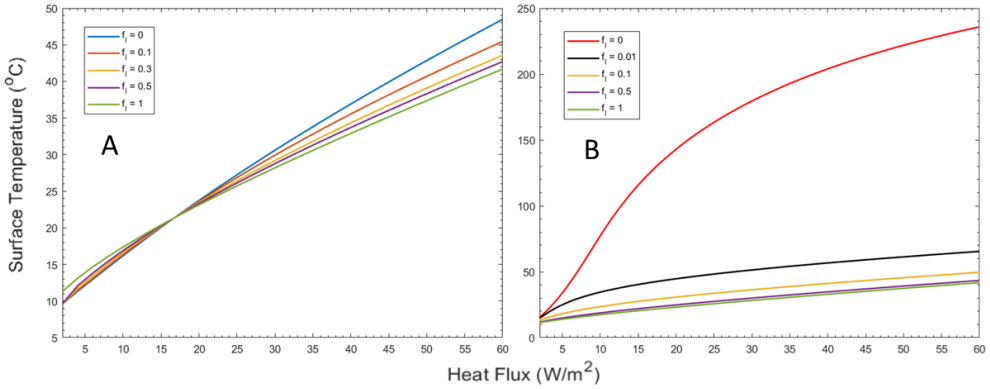

Figure 3. Average surface temperatures for Ignan Earth's while varying land fractions from 0 (ocean planet) to 1 (land planet). The ocean planet (blue curve) is the same reference case described in Fig. 2. In both plots, continental weathering is temperature dependent. However, in (A) seafloor weathering is temperature dependent, while in (B) seafloor weathering is temperature independent

our baseline planet from 0 - 1, shown in Fig. 3a. We see that continental weathering has the largest effect at high surface heat fluxes, lowering the predicted surface temperatures. Conversely, we find that the addition of continents increases the expected surface temperatures for low heat fluxes, though far less substantially. For temperature independent seafloor weathering we once again vary the land fraction from 0 - 1, shown in Fig. 3b.

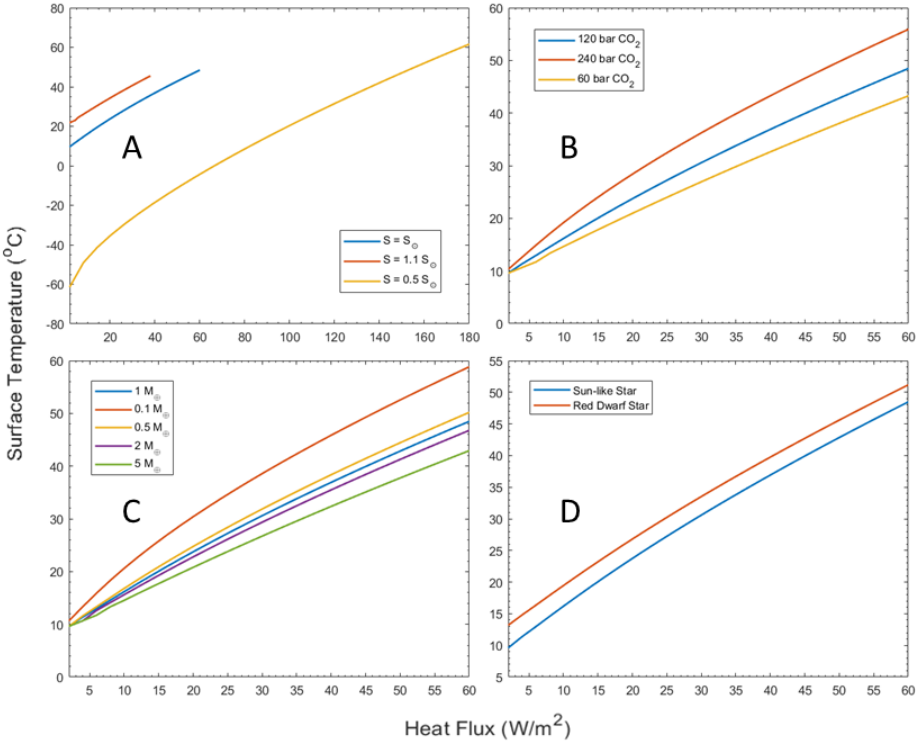

Figure 4. Average surface temperatures for Ignan Earth's while varying different properties. The blue curve is the same reference case in each plot, described in Fig. 2. (A) Varying solar insolation as a proxy for different locations within the habitable zone of a Sun-like star. These temperatures are calculated out to the geothermal heat flux that would trigger a runaway greenhouse, given that solar insolation + geothermal heat flux = total heat flux, and runaway greenhouse limit is a heat flux of 300 W m^{-2}. (B) Varying total amounts of carbon in the system. (C) Varying the simulated Ignan Earth mass. (D) Simulating an Ignan Earth around a red dwarf star receiving a stellar flux of 0.8 $S_{\odot}$ with a planetary albedo of 0.1.

When seafloor weathering is temperature independent, there is no temperature-induced negative feedback on CO_2, and thus no stabilizing effect acts to moderate the surface temperature, resulting in an inhospitable climate even at intermediate surface heat fluxes for low exposed land fractions. However, these inhospitable climates are replaced with hospitable ones once enough exposed continents are present for kinetically-limited continental weathering to dominate. Kinetically-limited weathering is temperature dependent, thus providing that temperature-induced negative feedback, stabilizing the climate at a temperate level.

Altering the location of our simulated Ignan Earth within the standard Habitable Zone, the total solar insolation will change, but so will the maximum geothermal heat flux needed to reach the Runaway Greenhouse Limit. We simulate the same Ignan Earth in the inner and outer Habitable Zone at 1.1 $S_{\odot}$ and 0.5 $S_{\odot}$, with the resulting surface temperatures shown in Fig. 4a. As expected, pushing the planet closer to the inner edge of the Habitable Zone increases the predicted surface temperatures, while pushing the planet farther out decreases the predicted temperatures. The Circumstellar Habitable Zone is the region around a star where it is possible for a planet to experience habitable

conditions, given the right atmospheric greenhouse gas concentrations. However, this does not mean that a planet will have the right concentrations. For the planet receiving a stellar insolation of 0.5 $S_{\odot}$, the greenhouse effect of the predicted CO_2 concentrations will not be sufficient to bring the average surface temperatures above the freezing point of water without extremely high geothermal heat fluxes (above 65 W m^{-2}).

As this model relies on CO_2 as the primary greenhouse gas that regulates surface temperature, the total content of carbon in the system will change the equilibrium CO_2 concentration in the atmosphere for any given geothermal heat flux. We explore variations in total CO_2 by taking the initial simulation result (Fig. 2) with total carbon contents of 2x and 0.5x our nominal value of 120 bars, seen in Fig. 4b. The results are as expected, with higher carbon contents leading to greater atmospheric CO_2 concentrations and thus higher predicted surface temperatures, and with lower carbon contents leading to lower predicted surface temperatures. However, these temperature variations are not significant enough to change the overall habitability of the planet.

In addition, we explore a wide range of planetary masses, as shown in Fig. 4c, where we find the predicted surface temperatures do not change significantly, especially for lower heat fluxes. The planet properties used in calculating the results in Fig. 4c are shown in Table 2. Like changes in overall carbon content, varying the mass of the planet causes relatively small changes in the predicted surface temperatures, especially at low geothermal heat fluxes and thus does not impact the overall habitability of the planet.

Another variation to consider is that of the star type the planet orbits, specifically red dwarf stars (known as M-dwarfs). It is around these stars that geothermal heat fluxes necessary for Ignan Earths might be possible through tidal heating. M-dwarfs are significantly cooler than Sun-like stars, meaning that their stellar spectrum will be dominated by infrared light. As both CO_2 and H_2O are stronger absorbers in infrared wavelengths than visible wavelengths, and materials such as water, rock, ice and clouds are less reflective in these wavelengths, planets around M-dwarfs will absorb far more of their host stars light than planets around Sun-like stars. Taking these factors into account, an Earth-like planet's albdeo would be reduced from our adopted nominal value of approximately 0.3 to values ranging from 0.17 (Joshi & Haberle, 2012) to 0.1 (Kopparapu et al., 2013). This difference in stellar spectra also alters the boundaries of the habitable zone, pushing the inner edge from 1.1 $S_{\odot}$ to 0.85 $S_{\odot}$. We simulate an Earth-like planet near the inner edge of the habitable zone of an M-dwarf star by by setting the solar insolation to 0.8 $S_{\odot}$ and the albedo to 0.1, comparing it to the results of the first simulation (see Fig. 4d). We find the predicted surface temperatures increased by less than 5 °C across the entire explored range of geothermal heat fluxes.

However, actual planets in the habitable zones around M-dwarf stars are likely to be tidally locked. This can cause their albedos to be higher than that of Earth, as the continuous stellar fluxes on their sub-stellar points may drive significant atmospheric convection and thus cloud formation, resulting in extensive cloud coverage. Yang et al. (2013) describes how albedos for such planets can reach up to 0.6. With such an albedo, our model predicts surface temperatures in the -50 to -80 °C range, which is likely not realistic. The high albedos proposed by Yang et al. (2013) come as the result of 3D GCM models of the planet's atmosphere, where the clouds produced by the extreme convective potential are caused by high stellar insolation localized to one region of the planet. An Ignan Earth will have a significant geothermal heat flux in addition to the stellar flux, and this geothermal flux would be spread uniformly across the planet. In order to understand the effects this would have on such a planet's climate would require using a 3D GCM model and including a significant geothermal heat flux.

Table 3. Parameters used in Ignan Earth climate model described in Sec. 3.

Parameter	Symbol	Value	Units
Henrian solubility constant of CO_2 in H_2O	K_H	235.48	bar
Water content of the ocean	p_{H_2O}	269	bar
Molar mass of H_2O	μ_{H_2O}	18.02	g mol^{-1}
Molar mass of CO_2	μ_{CO_2}	44.1	g mol^{-1}
Latent heat of H_2O	L_w	2469	J g^{-1}
Reference saturation vapor pressure	P^*_{sat}	610	Pa
Saturation vapor pressure reference temperature	T_{sat}	273	K
Reference surface temperature	T_{ref}	285	K
Reference effective temperature	T^*_{eq}	254	K
Reference spreading ridge velocity	$v_\oplus$	1.58×10^{-9}	m s^{-1}
Reference seafloor weathering rate	W^E_{sea}	12	bar Gyr^{-1}
Reference continental weathering rate	W^E_{kin}	53	bar Gyr^{-1}
CO_2 seafloor weathering scaling factor	α	0.23	
Velocity ratio scaling factor	β	1 - 0.5	
P_{sat} scaling factor	γ	0.3	
CO_2 continental weathering scaling factor	δ	0.55	
Crustal thickness	d_{bas}	4000	m
Mantle density	ρ_m	4000	kg m^{-3}
Mantle specific heat	C_p	1000	J K kg^{-1}
Mantle latent heat	L_m	4×10^5	J kg^{-1}
Temperature of erupted melt	T_{melt}	1625	K
CO_2 equilibrium partial pressure	P_E	0.01	bar
Activation energy	E	3×10^5	J kg^{-1}
CO_2 fraction outgassed	f_{gas}	0.1	
Land fraction	f_l	0 - 1	
Land fraction of the modern Earth	f^*_l	0.3	
Crustal surface density	ρ_{cont}	3000	kg m^{-3}
Fraction of reactable ions in crust	χ_{cc}	0.08	
Average molar mass of reactable elements in crust	m_{cc}	32	g mol^{-1}
Physical erosion rate	E_{rate}	10^{-2}	m yr^{-1}

4 Ignan Earth's in the Universe

Tidal dissipation is the most likely source of geothermal heating for potential Ignan Earths. This implies the planet orbits an M dwarf star, as only they have low enough stellar fluxes for their habitable zones to be close enough to allow a fast enough mean orbital motion of the planet for tidal heating to become significant. In addition to a short orbital period, there are numerous other factors needed for a world to experience high tidal heating. One of the most pressing is that of a non-zero eccentricity. However, the energy released due to tidal heating comes from the orbit of the planet, and thus internal heating comes at the cost of orbital eccentricity. On its own, tidal dissipation will circularize the orbit on any planet. The simplest way to overcome this and thus allow a planet to maintain a non-zero eccentricity and experience continuous tidal heating is for the planet to be in or near resonance with the orbits of other planets in the system, as Io is with Europa and Ganymede in the Jovian system (Luger et al., 2017).

McIntyre (2022) defines an optimal tidal heating zone between 40 mW m^{-2} and 300 W m^{-2}, where the lower limit is set by the minimum internal heat flux necessary to allow for mobile lid plate tectonics. As we have defined them here, Ignan Earth's would be found in the overlap of the circumstellar habitable zone and a more constrained range

of McIntyre (2022)'s tidal heating zone, extending down to 2 W m^{-2}. This overlap is shown in Fig. 4 by McIntyre (2022), and as the tidal heating zone for an Ignan Earth is narrower than the one shown in the figure, Ignan Earths would only be found in cases where there is substantial overlap between the two zones. Such overlap can be found in planets with masses greater than 0.5 $M_\oplus$ and with eccentricities of 0.1 and above. However, overlap is negligible or nonexistent for less massive worlds and those with eccentricities at or below 0.01.

4.1 Candidate Ignan Earths

Determining the tidal heating rates of exoplanets is a challenging task, as it requires knowledge of a wide variety of factors about the planets and their planetary system that are often unconstrained. While the planetary size, mass and mean orbital motion might be well known, large uncertainties often exist in the orbital eccentricity. In addition, the dissipation of tidal energy within the planet depends on the material properties and structure of the planet, which are also highly unconstrained. Different studies have attempted to calculate the tidal heating for some notable habitable zone M-dwarf planets using different models of tidal dissipation.

The TRAPPIST-1 system is one of the most well known potentially habitable M-dwarf systems, and consequently has been well studied. Numerous sources have estimates for the tidal heat fluxes of the systems seven planets. TRAPPIST-1b is estimated to have heat fluxes ranging from that of Io up to 10 W m^{-2} (Luger et al., 2017), meaning it is a Super Io candidate. However, the two innermost TRAPPIST-1 planets are inside the circumstellar habitable zone, meaning they are not Ignan Earths. Looking at the habitable zone planets, McIntyre (2022) estimates the tidal heating fluxes of TRAPPIST-1 d, e and f to be 1.27 W m^{-2}, 100 mW m^{-2} and 70 mW m^{-2}, respectively, whereas Bolmont et al. (2020) has differing values depending of the interior structure model used for each planet. For TRAPPIST-1e, they find a heat flux of 22 - 36 mW m^{-2} for the multi-layer and layer averaged models, and 1.5 - 2.4 W m^{-2} according to the homogeneous model. For TRAPPIST-1 f they calculate 25 - 34 mW m^{-2} for the multi-layer and layer averaged models, and 130 - 400 mW m^{-2} according to the homogeneous model. This is similar to the calculations done by Barr et al. (2018), where they found the tidal heating rates of TRAPPIST-1 d - f to be 140 - 180 mW m^{-2}. Regardless, even the most optimistic models predict the tidal heat fluxes barely reach those needed to be considered an Ignan Earth, making the habitable zone TRAPPIST-1 planets unlikely Ignan Earth candidates.

Other M-dwarf systems possess planets that are far more likely to be Ignan Earths. Teegarden's Star c is the outermost of the two known habitable zone Earth-massed planets within the system, and has an estimated tidal heat flux of 5.98 W m^{-2} (McIntyre, 2022), making it a prime Ignan Earth candidate. A similar candidate is Ross 128 b with an estimated tidal heat flux of 8.02 W m^{-2} (McIntyre, 2022). Even larger heat fluxes are calculated for Proxima Centauri b and GJ 1061 d, with values of 33.31 W m^{-2} and 42.28 W m^{-2}, respectively (McIntyre, 2022), making both of these worlds extreme Ignan Earth candidates. Some planets have simulated tidal heat fluxes in excess of the critical Tidal Venus limit set by Barnes et al. (2013), placing them outside the Ignan Earth tidal heating range. For example, Teegarden's Star b, the innermost known planet of Teegraden's Star system, has an estimated tidal heat flux of 392 W m^{-2} (McIntyre, 2022), likely making the planet a Tidal Venus. A similar fate is also probable for GJ 1061 c with an estimated tidal heat flux of 344 W m^{-2} (McIntyre, 2022), meaning both worlds have likely experienced a full runaway greenhouse.

5 Discussion

A terrestrial world should experience heat-pipe tectonics as long as the internal heat production is sufficient to maintain a mantle above the solidus temperature, thus ensuring a continuous supply of partial melt available for heat-pipe volcanism and thus sustain super-solidus convection (Moore et al., 2017). Moore et al. (2017) describes how all rocky worlds experience a heat-pipe tectonic phase after the solidification of their initial magma oceans, after which most will then transition to either a stagnant lid or mobile lid tectonic regime when internal heat production and mantle temperatures drop far enough for sub-solidus convection to dominate. As seen in Fig. 1, most of the explored range of geothermal heating is sufficient to maintain a mantle with continuous partial melt, regardless of planet mass, and thus any terrestrial world experiencing such internal heating will remain in a heat-pipe tectonic regime indefinitely and thus be classified as an Ignan Earth.

For Ignan Earth's powered by tidal heating, we assume a heat-pipe, vertical cycling tectonic regime and not a mobile lid regime. However, McIntyre (2022) indicates that enough tidal stress can provide sufficient lateral force on the crust to initiate subduction and thus force a planet into a mobile lid regime. Our model does not assume a mobile lid regime, or any type of hybrid mobile lid and heat-pipe tectonic system, therefore our model does not apply to any tidally induced mobile lid world. However, our model should still be widely applicable, as out of a sample of 767 terrestrial exoplanets studied by McIntyre (2022), only 28 % exceeded the threshold of tidal stress and are predicted to be in a mobile lid regime. Their data set includes numerous planets that are both in the habitable zone and have the optimal tidal heating rates to be Ignan Earths while not enough tidal stress to have mobile lid tectonics.

5.1 Climate Model Limitations

Even for terrestrial planets with continuous partial melt in their mantles that experience only heat-pipe tectonics, there are other limitations that should be specified. Our climate model does not take into account the transition to a runaway greenhouse, as we simply end the simulations at the 300 W/m^2 cutoff. It is possible that, in reality, the average surface temperature could rise distinctly as the critical heat flux is approached. Therefore our model likely underpredicts the average surface temperature when the total heat flux is near the Runaway Greenhouse Limit. However, this weakness in the model is probably not a problem for describing real Ignan Earths, as such worlds are very unlikely to have geothermal heat fluxes that extreme.

Underpredictions are also likely to occur for cold planets in the outer reaches of their stars habitable zone with low geothermal heat fluxes. As seen in Fig. 4a, an Ignan Earth at $0.5S_{\odot}$ will have surface temperatures far below freezing for low heat flux values. Our model assumes weathering occurs regardless of temperature, but in reality, low enough global temperatures will likely cut off the ocean from the atmosphere through a global glaciation, thus preventing seafloor weathering from occurring. In this case, CO_2 will build up in the atmosphere to keep the planet warm enough for at least some ocean to be ice free, allowing for atmosphere-ocean CO_2 exchange to occur, thus permitting seafloor weathering. Our model again underpredicts these surface temperatures, and a realistic temperature profile would flatten as it entered the -45°C to -70 °C range, the range of temperature predicted for a Snowball Earth (Micheels & Montenari, 2008).

One of the factors that influence the seafloor weathering rate is the resurfacing velocity. The normalizing factor ω in Eq. 24 was initially assumed to be 1, but if calculated, the value of ω varies from 0.2 - 6 in the 2 - 60 W/m^2 heat flux range, reaching values near 6 at 60 W/m^2. As this is a multiplicative factor when calculating the weathering rate, the highest values would increase the weathering rate, lowering the final atmospheric CO_2 content and thus lowering the final average global temperature by ap-

proximately 6 °C. At the other extreme, a value of 0.2 would decrease the rate of CO_2 removal from the atmosphere, yielding higher concentrations overall and a higher average temperature, but by less than 2 °C. However, this is assuming the scaling factor β has the typical value of 1 (Valencia et al., 2018). For a value of 0.5, as suggested by Krissansen-Totton and Catling (2017), the value of ω varies less than a factor of 2, causing an even smaller final temperature variations than when $\beta = 1$. Overall, these temperature variations are not significant enough to change the overall habitability of the simulated Ignan Earth.

Another possible limit to our Ignan Earth climate model is the possible inhibition of carbon return to the atmosphere due to volatile overpressure. As magma rises to the surface, the pressure experienced by the melt will decrease. The amount of dissolved CO_2 in the melt is determined in part by the pressure, and as that pressure decreases, the maximum CO_2 able to be dissolved will also decrease. Once a critical pressure is reached, the magma will become saturated and the CO_2 will degas to the atmosphere-ocean reservoir. However, for an Earth-mass planet, a 100 km deep ocean will increase the overall pressure of the ocean floor and underlying crust such that the CO_2 never reaches the critical degassing pressure. With a deep enough ocean, the resulting overpressure could cut off the means by which CO_2 is returned to the atmosphere, preventing this climate feedback cycle for taking place. For example, Kite et al. (2009) shows how an ocean 100 km deep on an Earth-mass planet will prevent CO_2 degassing from erupting melt containing 0.5 wt% CO_2. Going further, if an Earth-mass planet has surface water of over 40 Earth-oceans, the overpressure is high enough to raise the solidus temperature of the mantle such that no partial melting is possible, preventing heat-pipe tectonics from occurring at all (Kite et al., 2009). In either case, our model would no longer be applicable.

5.2 Geothermal Heating Model Limitations

In our model, we assume the mantle is homogeneous and any partial melt will be evenly distributed amongst the solids in a "magmatic sponge." However, recent work by Miyazaki and Stevenson (2022) indicates that magmatic sponges are not always stable, and a phase separation between the melt and the solid could sometimes occur, leading to separate magma ocean layer above the rest of the solid mantle. A magmatic sponge of a certain melt fraction requires sufficient heating to sustain that melt fraction, otherwise the melt will percolate up, separating the magmatic sponge into a liquid layer above a solid layer. Measurements suggests Io has an upper mantle melt fraction up to 0.2 (Khurana et al., 2011), but Miyazaki and Stevenson (2022) indicates estimates for Io's tidal heating rates are not sufficient to sustain a magmatic sponge with that melt fraction, arguing for the existence of separated melt and solid layers within. This would decouple the surface of Io from the interior, like the icy surface of Europa is decoupled from the interior by a liquid water ocean. If correct, this could imply that Ignan Earth mantles with intermediate melt fractions might undergo a phase separation, resulting in subsurface magma oceans. If this is true about Io, it implies that a solid crust can remain buoyant and thus stable over geologic time on a liquid mantle. While this is completely contrary to our basic assumptions in Sec. 2, observations do show that the crust of Io is stable, and thus perhaps our assumptions of what is necessary for a stable crust are too restrictive.

Such concerns could be circumvented if we consider the source of internal heating for the Ignan Earth. If internal heating is caused by tidal dissipation, then it is important to consider how dissipative mantle material is. A magmatic sponge is an effective dissipator of tidal stress, while a magma ocean is a likely poor dissipator, due to the lower viscosity (Miyazaki & Stevenson, 2022). For this reason, a similar feedback phenomenon might take place in a phase-separating mantle as we found in our own mantle evolution model: Internal heating might push the mantle past a critical point, where the melt and solid phases separate. Once this occurs, the mantle is no longer as effective at dissipat-

ing heat, cooling of the interior until the two separate phases re-aggregate. In this way, a magma ocean layer might be prevented from persisting for the same reasons a mantle with a melt fraction of over 0.4 is prevented, as described in Sec. 2.2.

Our work also assumes heating would be uniformly distributed throughout the planet, but in reality this is likely not the case. Evidence suggests that most of the tidally dissipated heat in Io is deposited in the equatorial regions of the mantle, given the higher concentrations of volcanoes found in those regions (Hamilton et al., 2013). A non-homogeneous surface heat flux would not affect the results of this work, as our models involve averages over the whole planet. However, tidal dissipation does not always occur within the mantle: In the Earth-Moon system, most dissipation happens in Earth's surface oceans (Murray & Dermott, 2000). If this is true for planet with Ignan Earth-like tidal conditions and similar ocean-land configurations as Earth, most of the dissipation will not be in the mantle, meaning it will not contribute to the internal heating and thus prevent the planet from being an Ignan Earth.

If tidal heating is the primary pathway that a terrestrial planet can become an Ignan Earth, this might effect the extent of the Habitable Zone. Habitable Zones for Ignan Earths may differ from those of more conventional, terrestrial planets. The inner and outer edges of traditional habitable zones are defined by the runaway greenhouse limit (Nakajima et al., 1992; Goldblatt & Watson, 2012) and the maximum greenhouse limit (Kopparapu et al., 2013), respectively. The entirety of the habitable zone is calculated assuming the planets possesses the carbonate-silicate cycle. However, an Ignan Earth would have a modified cycle which could affect the locations of the inner and outer edges. As the outer edge is farther from the star, the semi-major axis would be larger and consequently the mean orbital motion of the planet would be significantly slower, resulting in a significantly weaker tidal force. Therefore, it is likely that M-dwarf terrestrial planets are more likely to be Ignan Earths near the inner edge of habitable zones rather than the outer edge.

6 Conclusion

We investigate the habitability of Ignan Earths using a two-part method: First, by performing a mantle thermal evolution model to determine the rheology of the mantle and thus assess the stability of the crust, and second, using a climate model to determine the average surface temperature and overall habitability of the planet. We find that the mantle will maintain a melt fraction below the critical threshold of 0.4 ensuring a solid rheological state and thus permitting a stable, buoyant crust to form and persist over geologic time. A solid rheology is maintained even under extreme internal heating through a negative feedback loop, where increasing the melt fraction beyond 0.4 and proceeding into a liquid rheology will drop the mantle viscosity by orders of magnitude, increasing the vigor of convection and thus heat loss, cooling the mantle back until the critical threshold is met and a solid rheology dominates again.

With a stable surface, we simulate climate on an Ignan Earth over varying internal heat flux. We model a vertical, heat-pipe tectonic regime with a global ocean where seafloor weathering absorbs CO_2 and sequesters it in the crust, vertical cycling brings it to the mantle where the eruption of melt through heat-pipe volcanism degases it back to the surface. CO_2 is partitioned between the atmosphere and global ocean, where the atmospheric component is used as a greenhouse gas in a climate model where in incoming energy flux is a sum of the solar radiation from above plus the geothermal radiation from below. From this we compute the average surface temperatures expected on these Ignan Earths and find them to not only be suitable for liquid water to exist, but comparable to climate conditions Earth has experienced in its past. Therefore, Ignan Earth's should be habitable in principle and thus should not be overlooked in future searches for habitable exoplanets.

Open Research Section

Models for this research can be found at (Reinhold & Schaefer, 2023a), while data sets can be found at (Reinhold & Schaefer, 2023b).

Acknowledgments

M.R. would like to thank professors Mathieu Lapotre and Bruce Macintosh for their assistance through the process of thesis writing, and we would also like to acknowledge professor Norman Sleep for his insight into the nature of heat transport though the crust.

References

Abe, Y. (1997, March). Thermal and chemical evolution of the terrestrial magma ocean. *Physics of the Earth and Planetary Interiors*, *100*(1), 27-39. doi: 10.1016/S0031-9201(96)03229-3

Alt, J. C., & Teagle, D. A. H. (1999, May). The uptake of carbon during alteration of ocean crust. , *63*(10), 1527-1535. doi: 10.1016/S0016-7037(99)00123-4

Barnes, R., Jackson, B., Greenberg, R., & Raymond, S. N. (2009, July). Tidal Limits to Planetary Habitability. , *700*(1), L30-L33. doi: 10.1088/0004-637X/700/1/L30

Barnes, R., Mullins, K., Goldblatt, C., Meadows, V. S., Kasting, J. F., & Heller, R. (2013). Tidal venuses: triggering a climate catastrophe via tidal heating. *Astrobiology*, *13*(3), 225–250.

Barr, A. C., Dobos, V., & Kiss, L. L. (2018, May). Interior structures and tidal heating in the TRAPPIST-1 planets. , *613*, A37. doi: 10.1051/0004-6361/201731992

Berner, R. A., Lasaga, A. C., & Garrels, R. M. (1983, September). The carbonate-silicate geochemical cycle and its effect on atmospheric carbon dioxide over the past 100 million years. *American Journal of Science*, *283*(7), 641-683. doi: 10.2475/ajs.283.7.641

Bolmont, E., Breton, S. N., Tobie, G., Dumoulin, C., Mathis, S., & Grasset, O. (2020, December). Solid tidal friction in multi-layer planets: Application to Earth, Venus, a Super Earth and the TRAPPIST-1 planets. Potential approximation of a multi-layer planet as a homogeneous body. , *644*, A165. doi: 10.1051/0004-6361/202038204

Boukaré, C. E., Parmentier, E. M., & Parman, S. W. (2018, June). Timing of mantle overturn during magma ocean solidification. *Earth and Planetary Science Letters*, *491*, 216-225. doi: 10.1016/j.epsl.2018.03.037

Bower, D. J., Kitzmann, D., Wolf, A. S., Sanan, P., Dorn, C., & Oza, A. V. (2019, November). Linking the evolution of terrestrial interiors and an early outgassed atmosphere to astrophysical observations. , *631*, A103. doi: 10.1051/0004-6361/201935710

Davies, G. F. (2007). *Thermal Evolution of the Mantle* (Vol. 9; G. Schubert, Ed.). Frisco, CO: Elsevier. doi: 10.1016/B978-044452748-6.00145-0

Driscoll, P. E., & Barnes, R. (2015, September). Tidal Heating of Earth-like Exoplanets around M Stars: Thermal, Magnetic, and Orbital Evolutions. *Astrobiology*, *15*(9), 739-760. doi: 10.1089/ast.2015.1325

Elkins-Tanton, L. T. (2008, July). Linked magma ocean solidification and atmospheric growth for Earth and Mars. *Earth and Planetary Science Letters*, *271*(1-4), 181-191. doi: 10.1016/j.epsl.2008.03.062

Fei, H., Yamazaki, D., Sakurai, M., Miyajima, N., Ohfuji, H., Katsura, T., & Yamamoto, T. (2017, June). A nearly water-saturated mantle transition zone inferred from mineral viscosity. *Science Advances*, *3*, e1603024. doi: 10.1126/sciadv.1603024

Foley, B. J. (2015, October). The Role of Plate Tectonic-Climate Coupling and Exposed Land Area in the Development of Habitable Climates on Rocky Planets. , *812*(1), 36. doi: 10.1088/0004-637X/812/1/36

Fontaine, F. J., Olive, J.-A., Cannat, M., Escartin, J., & Perol, T. (2011, July). Hydrothermally-induced melt lens cooling and segmentation along the axis of fast- and intermediate-spreading centers. , *38*(14), L14307. doi: 10.1029/2011GL047798

Goldblatt, C., & Watson, A. J. (2012, September). The runaway greenhouse: implications for future climate change, geoengineering and planetary atmospheres. *Philosophical Transactions of the Royal Society of London Series A*, *370*(1974), 4197-4216. doi: 10.1098/rsta.2012.0004

Hamilton, C. W., Beggan, C. D., Still, S., Beuthe, M., Lopes, R. M. C., Williams, D. A., ... Wright, W. (2013, January). Spatial distribution of volcanoes on Io: Implications for tidal heating and magma ascent. *Earth and Planetary Science Letters*, *361*, 272-286. doi: 10.1016/j.epsl.2012.10.032

Hirschmann, M. M. (2018, November). Comparative deep Earth volatile cycles: The case for C recycling from exosphere/mantle fractionation of major (H_2O, C, N) volatiles and from H_2O/Ce, CO_2/Ba, and CO_2/Nb exosphere ratios. *Earth and Planetary Science Letters*, *502*, 262-273. doi: 10.1016/j.epsl.2018.08.023

Inglis, G. N., Bragg, F., Burls, N. J., Cramwinckel, M. J., Evans, D., Foster, G. L., ... Pancost, R. D. (2020, October). Global mean surface temperature and climate sensitivity of the early Eocene Climatic Optimum (EECO), Paleocene-Eocene Thermal Maximum (PETM), and latest Paleocene. *Climate of the Past*, *16*(5), 1953-1968. doi: 10.5194/cp-16-1953-2020

Joshi, M. M., & Haberle, R. M. (2012, January). Suppression of the Water Ice and Snow Albedo Feedback on Planets Orbiting Red Dwarf Stars and the Subsequent Widening of the Habitable Zone. *Astrobiology*, *12*(1), 3-8. doi: 10.1089/ast.2011.0668

Kasting, J. F., Whitmire, D. P., & Reynolds, R. T. (1993, January). Habitable Zones around Main Sequence Stars. , *101*(1), 108-128. doi: 10.1006/icar.1993.1010

Khurana, K. K., Jia, X., Kivelson, M. G., Nimmo, F., Schubert, G., & Russell, C. T. (2011, June). Evidence of a Global Magma Ocean in Io's Interior. *Science*, *332*(6034), 1186. doi: 10.1126/science.1201425

Kislyakova, K. G., Fossati, L., Johnstone, C. P., Noack, L., Lüftinger, T., Zaitsev, V. V., & Lammer, H. (2018, May). Effective Induction Heating around Strongly Magnetized Stars. , *858*(2), 105. doi: 10.3847/1538-4357/aabae4

Kite, E. S., Manga, M., & Gaidos, E. (2009, August). Geodynamics and Rate of Volcanism on Massive Earth-like Planets. , *700*(2), 1732-1749. doi: 10.1088/0004-637X/700/2/1732

Kopparapu, R. K., Ramirez, R., Kasting, J. F., Eymet, V., Robinson, T. D., Mahadevan, S., ... Deshpande, R. (2013, March). Habitable Zones around Main-sequence Stars: New Estimates. , *765*(2), 131. doi: 10.1088/0004-637X/765/2/131

Krissansen-Totton, J., & Catling, D. C. (2017, May). Constraining climate sensitivity and continental versus seafloor weathering using an inverse geological carbon cycle model. *Nature Communications*, *8*, 15423. doi: 10.1038/ncomms15423

Lainey, V., Arlot, J.-E., Karatekin, Ö., & van Hoolst, T. (2009, June). Strong tidal dissipation in Io and Jupiter from astrometric observations. , *459*(7249), 957-959. doi: 10.1038/nature08108

Lebrun, T., Massol, H., ChassefièRe, E., Davaille, A., Marcq, E., Sarda, P., ... Brandeis, G. (2013, June). Thermal evolution of an early magma ocean in interaction with the atmosphere. *Journal of Geophysical Research (Planets)*, *118*(6), 1155-1176. doi: 10.1002/jgre.20068

Luger, R., Sestovic, M., Kruse, E., Grimm, S. L., Demory, B.-O., Agol, E., ... Queloz, D. (2017, June). A seven-planet resonant chain in TRAPPIST-1. *Nature Astronomy*, *1*, 0129. doi: 10.1038/s41550-017-0129

Marty, B. (2012, January). The origins and concentrations of water, carbon, nitrogen and noble gases on Earth. *Earth and Planetary Science Letters*, *313*, 56-66. doi: 10.1016/j.epsl.2011.10.040

Maurice, M., Tosi, N., Samuel, H., Plesa, A.-C., Hüttig, C., & Breuer, D. (2017, March). Onset of solid-state mantle convection and mixing during magma ocean solidification. *Journal of Geophysical Research (Planets)*, *122*(3), 577-598. doi: 10.1002/2016JE005250

McIntyre, S. R. N. (2022, June). Tidally driven tectonic activity as a parameter in

exoplanet habitability. , *662*, A15. doi: 10.1051/0004-6361/202141112

Micheels, A., & Montenari, M. (2008, January). A snowball Earth versus a slushball Earth: Results from Neoproterozoic climate modeling sensitivity experiments. *Geosphere*, *4*(2), 401. doi: 10.1130/GES00098.1

Miyazaki, Y., & Stevenson, D. J. (2022). A subsurface magma ocean on io: Exploring the steady state of partially molten planetary bodies. *arXiv preprint arXiv:2211.06945*.

Moore, W. B., Simon, J. I., & Webb, A. A. G. (2017, September). Heat-pipe planets. *Earth and Planetary Science Letters*, *474*, 13-19. doi: 10.1016/j.epsl.2017.06.015

Moore, W. B., & Webb, A. A. G. (2013, September). Heat-pipe Earth. , *501*(7468), 501-505. doi: 10.1038/nature12473

Morison, A., Labrosse, S., Deguen, R., & Alboussière, T. (2019, June). Timescale of overturn in a magma ocean cumulate. *Earth and Planetary Science Letters*, *516*, 25-36. doi: 10.1016/j.epsl.2019.03.037

Murray, C. D., & Dermott, S. F. (2000). *Solar System Dynamics*.

Nakajima, S., Hayashi, Y.-Y., & Abe, Y. (1992, December). A study on the 'runaway greenhouse effect' with a one-dimensional radiative-convective equilibrium model. *Journal of Atmospheric Sciences*, *49*(23), 2256-2266. doi: 10.1175/1520-0469(1992)049⟨2256:ASOTGE⟩2.0.CO;2

Nishi, M., Irifune, T., Tsuchiya, J., Tange, Y., Nishihara, Y., Fujino, K., & Higo, Y. (2014, March). Stability of hydrous silicate at high pressures and water transport to the deep lower mantle. *Nature Geoscience*, *7*, 224-227. doi: 10.1038/ngeo2074

O'Connor, L. K., Robinson, S. A., Naafs, B. D. A., Jenkyns, H. C., Henson, S., Clarke, M., & Pancost, R. D. (2019, April). Late Cretaceous Temperature Evolution of the Southern High Latitudes: A TEX86Perspective. *Paleoceanography and Paleoclimatology*, *34*(4), 436-454. doi: 10.1029/2018PA003546

O'Neill, C., & Roberts, N. M. (2018). Lid tectonics. preface. *Geoscience Frontiers*, *9*(1), 1–2.

O'Reilly, T. C., & Davies, G. F. (1981, April). Magma transport of heat on Io: A mechanism allowing a thick lithosphere. , *8*(4), 313-316. doi: 10.1029/GL008i004p00313

Peslier, A. H., Schönbächler, M., Busemann, H., & Karato, S.-I. (2017, October). Water in the Earth's Interior: Distribution and Origin. , *212*, 743-810. doi: 10.1007/s11214-017-0387-z

Reinhold, M., & Schaefer, L. (2023a). Ignan Earth Codes. Stanford Digital Repository.. Retrieved from `https://purl.stanford.edu/jt673zb0893` doi: 10.25740/jt673zb0893

Reinhold, M., & Schaefer, L. (2023b). Ignan Earth Data. Stanford Digital Repository.. Retrieved from `https://purl.stanford.edu/gc321qs2451` doi: 10.25740/gc321qs2451

Schaefer, L., Wordsworth, R. D., Berta-Thompson, Z., & Sasselov, D. (2016, October). Predictions of the Atmospheric Composition of GJ 1132b. , *829*(2), 63. doi: 10.3847/0004-637X/829/2/63

Schmandt, B., Jacobsen, S. D., Becker, T. W., Liu, Z., & Dueker, K. G. (2014, June). Dehydration melting at the top of the lower mantle. *Science*, *344*(6189), 1265-1268. doi: 10.1126/science.1253358

Selsis, F., Kasting, J. F., Levrard, B., Paillet, J., Ribas, I., & Delfosse, X. (2007, December). Habitable planets around the star Gliese 581? , *476*(3), 1373-1387. doi: 10.1051/0004-6361:20078091

Shields, A. L., Ballard, S., & Johnson, J. A. (2016, December). The habitability of planets orbiting M-dwarf stars. , *663*, 1. doi: 10.1016/j.physrep.2016.10.003

Sleep, N. H., Zahnle, K. J., & Lupu, R. E. (2014, August). Terrestrial aftermath of the Moon-forming impact. *Philosophical Transactions of the Royal Society of*

London Series A, *372*(2024), 20130172-20130172. doi: 10.1098/rsta.2013.0172

Solomatov, V. (2007). *Magma Oceans and Primordial Mantle Differentiation* (Vol. 9; G. Schubert, Ed.). Frisco, CO: Elsevier. doi: 10.1016/B978-044452748-6.00141-3

Tierney, J. E., Zhu, J., King, J., Malevich, S. B., Hakim, G. J., & Poulsen, C. J. (2020, August). Glacial cooling and climate sensitivity revisited. , *584*(7822), 569-573. doi: 10.1038/s41586-020-2617-x

Valencia, D., Tan, V. Y. Y., & Zajac, Z. (2018, April). Habitability from Tidally Induced Tectonics. , *857*(2), 106. doi: 10.3847/1538-4357/aab767

Walker, J. C. G., Hays, P. B., & Kasting, J. F. (1981, October). A negative feedback mechanism for the long-term stabilization of the earth's surface temperature. , *86*, 9776-9782. doi: 10.1029/JC086iC10p09776

Yang, J., Cowan, N. B., & Abbot, D. S. (2013, July). Stabilizing Cloud Feedback Dramatically Expands the Habitable Zone of Tidally Locked Planets. , *771*(2), L45. doi: 10.1088/2041-8205/771/2/L45

Zeng, L., Jacobsen, S. B., Sasselov, D. D., Petaev, M. I., Vanderburg, A., Lopez-Morales, M., ... Wordsworth, R. D. (2019, May). Growth model interpretation of planet size distribution. *Proceedings of the National Academy of Science*, *116*(20), 9723-9728. doi: 10.1073/pnas.1812905116